KERNFORSCHUNGSANLAGE JÜLICH GmbH

Institut für Plasmaphysik
Association EURATOM - KFA

Combined Interferometric and Polarimetric Diagnostics for TEXTOR

by

H. Soltwisch

Jül - 1638
Januar 1980
ISSN 0366-0885

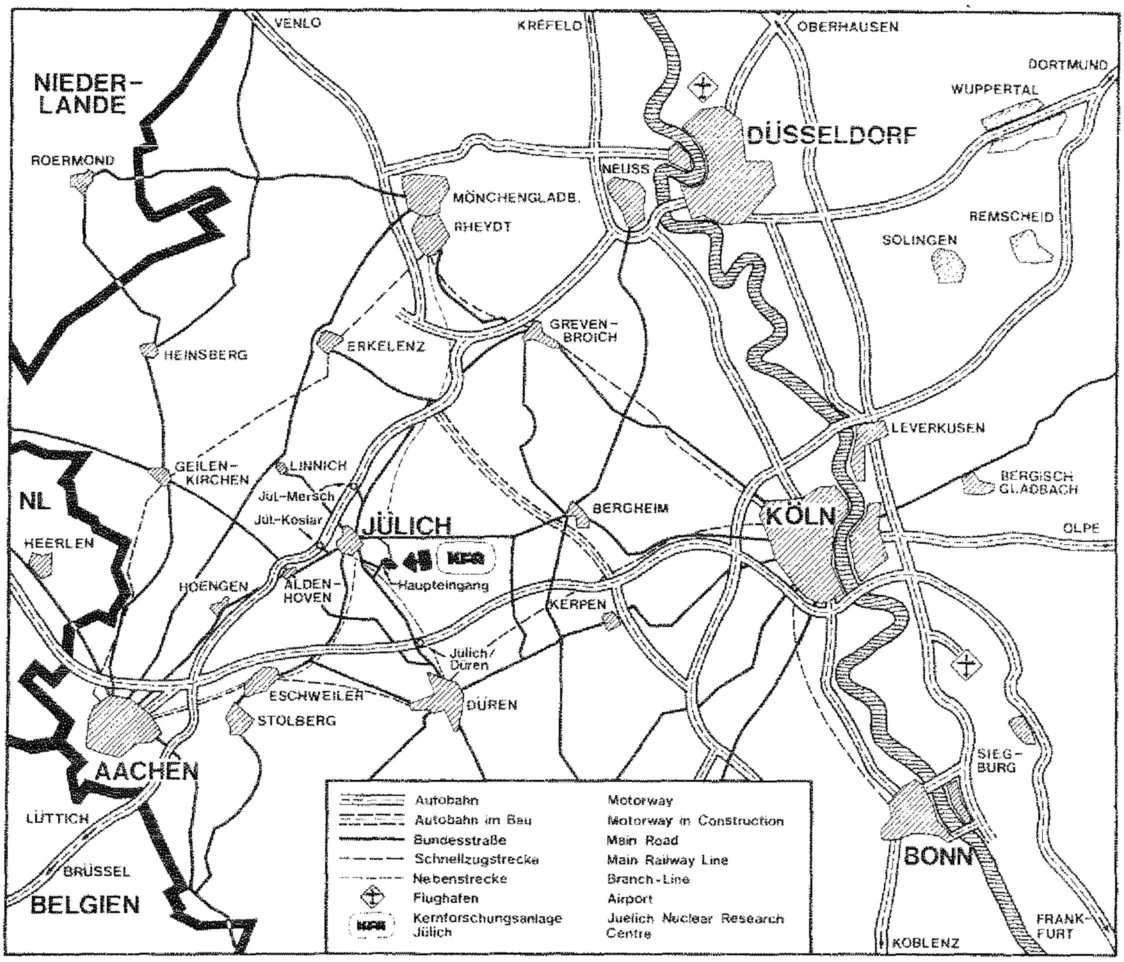

Als Manuskript gedruckt

Berichte der Kernforschungsanlage Jülich – Nr. 1638

Institut für Plasmaphysik Jül - 1638

Zu beziehen durch: ZENTRALBIBLIOTHEK der Kernforschungsanlage Jülich GmbH,
Jülich, Bundesrepublik Deutschland

Combined Interferometric and Polarimetric Diagnostics for TEXTOR

by

H. Soltwisch

Abstract

A method for combining Faraday rotation measurements with a phase modulated HCN interferometer is described, which enables the simultaneous determination of the line integrals $\int N_e ds$ and $\int N_e \cdot B_{\parallel} \cdot ds$. Extended to a multichannel system this technique should allow to investigate the distributions of electron density and poloidal magnetic field in a Tokamak plasma. We discuss the principle of operation and appropriate evaluation of measured data with regard to TEXTOR parameters and give an estimate for the expected experimental accuracy.

I. Introduction

The behaviour of a Tokamak plasma is for a great part determined by its electron density distribution and its current density profile, and a detailed knowledge of these parameters is essential for understanding fundamental problems as e.g. transport phenomena and plasma stability. Consequently, strong efforts have been made to develop techniques of measurement which allow for high accuracy and good temporal resolution. Concerning the determination of electron density, interferometry using microwave or far infrared radiation has become a routine method for all present-day and near-future Tokamaks, and a lot of publications deals with this technique and its sophisticated variations (an extensive survey on submillimeter interferometry has recently been given by Véron /1/). On the contrary, no measuring technique for current density profiles is well established up to now. A possible approach to this problem makes use of the close relation between current density distribution and resulting poloidal magnetic field inside the plasma. It is well known, that the plane of polarization of an electromagnetic wave, as it passes along the field lines in a magnetized plasma, is rotated due to the Faraday effect. The amount of rotation can be measured by means of polarimetric techniques, providing informations on the internal field and hence on the current density profile. In principle, such a polarimetric device is operated with a linearly polarized beam of light traversing a poloidal plasma cross section perpendicular to the plasma current. Since the poloidal magnetic field $\vec{B}_p$ has a vector component $B_{p\parallel}$ parallel to the beam path, the plane of polarization rotates by the angle (De Marco, Segre /2/):

$$\alpha\ [\mathrm{deg}] = 1{,}50 \cdot 10^{-20}\, \lambda^2 \int_0^L N_e\, B_{p\parallel}\, ds \tag{1}$$

λ : probing wavelength in μm
N_e: electron density in cm^{-3}
$B_{p\parallel}$: magnetic field component in kG
L: probing chord length in cm

Strictly speaking, equ. (1) is only valid for a fully ionized collisionless plasma. Furthermore, linear birefringence (Cotton-Mouton effect) mainly arising from the toroidal magnetic field $\vec{B}_T$ normal to the beam is completely neglected. According to De Marco and Segre /2/ the latter is only permitted if the following condition is satisfied (see also Véron /1/):

$$B_T^2\, \overline{N}_e < 4{,}1 \cdot 10^{25}\, \lambda^{-3}\, L^{-1} \tag{2}$$

B_T : toroidal magnetic field in kG
$\overline{N}_e = \frac{1}{L} \int_0^L N_e ds$: mean density along the probing chord

Putting numbers corresponding to TEXTOR parameters ($\overline{N}_e = 3 \cdot 10^{13}\ cm^{-3}$, B_T = 20 kG, L = 100 cm), equ. (2) yields an upper wavelength limit of 325 μm. This value is fairly close to 337 μm for which powerful and reliable HCN laser sources exist (Belland et al. /3/). Nevertheless, employing the HCN laser requires a slight correction of equ. (1) which will be discussed later on. But the expected Faraday rotation angles are rather small. To make an estimate, both the electron density distribution $N_e(r)$ and the current density profile j (r) are supposed to be parabolic with a peak density of $N_{eo} = 5 \cdot 10^{13}\ cm^{-3}$ and a total current of 300 kA. It then follows from equ. (1) that the maximum angle of rotation is only 3,57 deg. Consequently, accurate measurements of Faraday rotation require somewhat elaborate techniques to yield high enough precision, and this may be one of the reasons why this method is not yet routinely applied. Moreover, the Faraday rotation angle is an integral quantity, and in order to derive the radial distribution j(r) it is necessary to probe the plasma along different chords in a multichannel device. But since electron and current density profiles are not always symmetric, the transformation of a measured rotation angle distribution to the distribution of current density may turn out to be difficult. In spite of these disadvantages Faraday rotation diagnostics is a promising approach to local magnetic field measurement, especially because none of the other methods (recently reviewed by Peacock /4/) has finally demonstrated its routine applicability.

The present report deals only with one of the above mentioned difficulties, namely the accurate determination of small rotation angles. The concept described here is a combination of a HCN laser interferometer first developed by Véron et al. /5/ for the TFR Tokamak and a sensitive heterodyne polarimeter proposed by Andrade /6/, which minimizes the instrumental equipment by using the same probing beams for both interferometric and polarimetric purposes. The following chapter deals with the principle of operation, then the interpretation of detector signals is discussed, and finally we analyze the error introduced to the rotation measurements by the Cotton-Mouton effect.

II. Principle of operation

The technical feasibility of Faraday rotation measurements under Tokamak conditions using 337 μm radiation has been demonstrated on TFR by Kunz et al. /7/. The authors employed a ferrite modulation method (Pieroni /8/, Dodel and Kunz /9/), which produced a probing beam with oscillating plane of polarization and permitted the use of phase sensitive detection locked onto the modulation frequency. However, this technique suffers from the low transmission of the ferrite modulator, which is a serious drawback especially in a multichannel device. Another method suggested by Dodel and Kunz /10/, but not yet tested under Tokamak conditions, operates with a continuously rotating plane of polarization in the probing beam and enables simultaneous measurements of Faraday rotation and electron line density. Its main drawback is the necessity for sensitive low-noise detectors (for example liquid helium cooled InSb) and for beam splitters insensitive to polarization.

The arrangement to be described here was first proposed by Véron and Crenn /1/, and its feasibility has been proved in a preparatory experiment. The principle of operation is explained by refering to fig. 1. A linearly polarized monochromatic input beam passes through a beam splitter and is divided into two plane waves of equal intensities. The reflected part (reference beam) is then focussed on a rotating cylindrical grating (Véron /11/) and experiences a Doppler shift $\Delta\omega$, which depends on the rotating speed of the grating. Due to reflections at metallic surfaces the initial linear polarization becomes somewhat elliptic, and the major axis of the vibrational ellipse may be tilted by an angle ψ_r relative to the principle plane of fig. 1. Then the electric field of the reference wave is given by the real part of the complex vector

$$\vec{\mathbb{E}}_r = \begin{bmatrix} \mathbb{E}_{rp} \\ \mathbb{E}_{rs} \end{bmatrix} = a_r \cdot \exp[j(\omega + \Delta\omega)t] \begin{vmatrix} \cos\psi_r & \sin\psi_r \\ -\sin\psi_r & \cos\psi_r \end{vmatrix} \begin{bmatrix} 1 \\ j\cdot\varepsilon_r \end{bmatrix} \tag{3}$$

wherein the ellipticity $\varepsilon_r = \pm b_r/a_r$ is defined as the ratio of minor to major axis of the vibrational ellipse (the major axis a_r depends on the beam intensity I_r according to $a_r \sim \sqrt{I_r/(1+\varepsilon_r^2)}$; for the definition of p- and s-axes see fig. 1).

The probing beam traverses a poloidal plasma cross section and experiences a phase shift (e.g. Alpher and White /12/)

$$\Delta\varphi\,[\mathrm{rad}] = -2{,}82\cdot 10^{-17}\,\lambda \int_0^L N_e \cdot ds \tag{4}$$

and, of course, a Faraday rotation α according to equ. (1). As a matter of fact, the phase shift given by equ. (4) is valid only for ordinary mode propagation (i.e. electric field vector parallel to magnetic field lines inside the plasma). But for typical TEXTOR plasma parameters and a probing wavelength of 337 μm the refractivities of the ordinary and extraordinary modes (e.g. Heald and Wharton /13/) differ by less than 0,5 %, leading to a correspondingly small difference in phase shifts, which does not seriously affect the electron line density measurements. On the other hand, deviations from ordinary mode propagation introduce some ellipticity to the probing beam polarization, whereby the vibrational ellipse is rotated due to the Faraday effect (a more detailed analysis will be given in chapter IV). After having traversed the plasma cross section the probing beam passes through a halfwave plate, by which the p- and s-components of the electric field are interchanged. Then the complex field vector of the probing wave can be expressed as

$$\vec{\mathbb{E}}_p = \begin{bmatrix} \mathbb{E}_{pp} \\ \mathbb{E}_{ps} \end{bmatrix} = a_p \cdot \exp[j(\omega t - \Delta\varphi)] \begin{vmatrix} \cos\psi_p & \sin\psi_p \\ -\sin\psi_p & \cos\psi_p \end{vmatrix} \begin{bmatrix} -j\cdot\varepsilon_p \\ 1 \end{bmatrix}. \tag{5}$$

Next, probing and reference waves are recombined at a wire grid beam splitter (i.e. an array of free-standing parallel metal wires). Before we can write down the resulting electric fields we must briefly discuss the transmission and reflection properties of such a wire grid. A theoretical treatment on the basis of transmission line theory has been given by several authors (e.g. Marcuvitz /14/).

According to this concept the wire grid can be substituted by an equivalent electrical circuit, which is formed by a transmission line of impedance Z_o representing free space, shunted by an impedance jX_o representing the grid. The shunt is either a capacitance or an inductance depending on the polarization of the incident wave (see fig. 2). From transmission line theory the power reflectance is found to be (Möller and Rothschild /15/):

$$R = \frac{Z_o^2}{Z_o^2 + 4X_o^2} . \tag{6}$$

Since the equivalent circuit represents a lossless grid (because of the purely imaginary shunt impedance) the power transmittance results in

$$T = 1 - R = \frac{4X_o^2}{Z_o^2 + 4X_o^2} . \tag{7}$$

The phase shifts of the reflected and transmitted waves relative to the incident wave are given by

$$\phi_R = \pi - \arctan\frac{2X_o}{Z_o} = \pi - \arctan\sqrt{T/R}$$

$$\phi_T = \arctan\frac{Z_o}{2X_o} = \arctan\sqrt{R/T} \tag{8}$$

$$|\phi_R - \phi_T| = \pi/2$$

The grid to be used in the arrangement of fig. 1 has its wires parallel to the principle plane. The wire spacing is such that the p-component of an incident wave is divided into two p-waves of almost equal amplitude, which are phase shifted by $\phi_{R_p} = 3\pi/4$ and $\phi_{T_p} = \pi/4$, resp. (see fig. 2b; grids with these properties are manufactured by SPECAC Analytical Accessories /16/ using tungsten wires of 10 µm diameter and 152 µm spacing for a wavelength of 337 µm). For an s-wave with its electric field normal to the wires the grid is almost completely transparent ($T_s \approx 1$, $R_s \approx 0$; see fig. 2c). The reason is that the field cannot excite currents in the grid, if the diameter of the wires is small compared with the wavelength.

Returning to fig. 1 we will now calculate the electric field vectors after beam recombination using the grid characteristics given in fig. 2. We will first examine the interferometer beam. In plane I of fig. 1 the electric field is found to be

$$\vec{\mathbb{E}}_I = \begin{bmatrix} \mathbb{E}_{Ip} \\ \mathbb{E}_{Is} \end{bmatrix} = \begin{vmatrix} 1/\sqrt{2}\cdot\exp[j\cdot\pi/4] & 0 \\ 0 & 1 \end{vmatrix} \vec{\mathbb{E}}_p + \begin{vmatrix} 1/\sqrt{2}\cdot\exp[j\cdot 3\pi/4] & 0 \\ 0 & 0 \end{vmatrix} \vec{\mathbb{E}}_r \tag{9}$$

$\mathbb{E}_{Ip}$ and $\mathbb{E}_{Is}$, which contain the main components $\mathbb{E}_{rp}$ and $\mathbb{E}_{ps}$ of the reference and probing beam, are orthogonal and hence do not interfere, unless they are superimposed in a diagonal direction. Therefore they have to pass through an analyzer set at 45^0 relative to the p- and s-axes. The analyzer is also a wire grid but with small wire spacing in order to achieve high polarizing efficiency (SPECAC Analytical Accessories /16/ recommends a spacing of 25 µm for 337 µm wavelength, which reduces the transmission for "wrong" polarized radiation to less than 2 %). If we denote the analyzer transmission coefficients for "right" and "wrong" polarized waves by T_c and T_w resp. the electric field behind the analyzer (plane II in fig. 1) can be written as

$$\vec{\mathbb{E}}_{II} = \begin{bmatrix} \mathbb{E}_{IIc} \\ \mathbb{E}_{IIw} \end{bmatrix} = \begin{vmatrix} \sqrt{T_c/2}\ \exp[j\cdot\Phi_c] & -\sqrt{T_c/2}\ \exp[j\cdot\Phi_c] \\ \sqrt{T_w/2}\ \exp[j\cdot\Phi_w] & \sqrt{T_w/2}\ \exp[j\cdot\Phi_w] \end{vmatrix} \vec{\mathbb{E}}_I \tag{10}$$

(Note, that the c-w-coordinate system is rotated by 45^0 with respect to the previous p-s-system; Φ_c and Φ_w account for the phase shifts of the transmitted waves).

The wave defined by equ. (10) finally arrives at the interferometer detector whose output signal S_I is proportional to the beam intensity (for the sake of simplicity the constant of proportionality is henceforth omitted):

$$S_I = \vec{\mathbb{E}}_{II}\cdot\vec{\mathbb{E}}_{II}^{\times} \tag{11}$$

Using equations (9) and (10) the output signal results in

$$S_I = \left\{\frac{T_c+T_w}{4}\left[\vec{\mathbb{E}}_p\cdot\vec{\mathbb{E}}_p^{\times} + \mathbb{E}_{ps}\mathbb{E}_{ps}^{\times} + \mathbb{E}_{rp}\mathbb{E}_{rp}^{\times}\right] - \frac{T_c-T_w}{2}\,\mathrm{Re}\left[(1+j)\,\mathbb{E}_{pp}\mathbb{E}_{ps}^{\times}\right]\right\} + \dots$$
$$\dots + \left\{\frac{T_c+T_w}{2}\,\mathrm{Im}\left[\mathbb{E}_{pp}\mathbb{E}_{rp}^{\times}\right] + \frac{T_c-T_w}{2}\,\mathrm{Re}\left[(1-j)\,\mathbb{E}_{rp}\mathbb{E}_{ps}^{\times}\right]\right\} \tag{12}$$

The first curved brackets represent a constant background intensity dependent on the amplitude components of the probing and reference waves. The second brackets form the interference term which describes the interaction of the probing and reference waves as a function of their phase difference. Inserting the field components defined in equations (3) and (5) the interferometer signal can be expressed as

$$S_l = U_l + V_l \cdot \cos(\Delta\omega t + \Delta\varphi + \Phi_l) \tag{13}$$

The quantities U_l and V_l and the phase angle Φ_l depend on the polarization parameters (ε_p, ψ_p), (ε_r, ψ_r) and on the intensities I_p, I_r of the probing and reference beams. If the polarization parameters are small compared to unity (as will be the case under usual operational conditions), then U_l, V_l, and Φ_l are well approximated by

$$\begin{aligned} U_l/(T_c - T_w) &\approx (K - \psi_p - \varepsilon_p) \cdot I_p/2 + K \cdot I_r/4 \approx K(I_p/2 + I_r/4) \\ V_l/(T_c - T_w) &\approx \sqrt{[1 - K(\varepsilon_p + \psi_p)] \cdot I_p I_r/2} \approx \sqrt{I_p I_r/2} \\ \tan\Phi_l &\approx -(1 - K\psi_p)/(1 - K\varepsilon_p) \end{aligned} \tag{14}$$

wherein $K = (T_c+T_w)/(T_c-T_w)$ accounts for non-perfect analyzer characteristics.

It is important to note that the total phase shift observed in the interferometer signal consists of the sum of plasma phase shift $\Delta\varphi$ and phase angle Φ_l. However, variations of Φ_l due to linear plasma birefringence and Faraday effect are negligibly small compared with the corresponding values of $\Delta\varphi$. As can be estimated from equ. (14), five degrees of Faraday rotation ($\Delta\psi_p = 0{,}087$) cause a variation $\Delta\Phi_l < \pi/50$. On the other hand, five degrees of Faraday rotation observed with 337 µm radiation under TEXTOR conditions (I = 300 kA) require an electron line density of more than $3 \cdot 10^{15}$ cm^{-2}, and the resulting plasma phase shift amounts $\Delta\varphi = 9\pi$. A similar estimate holds for variations of the ellipticity ε_p.

Let us now examine the polarimeter beam of fig. 1. Its electric field in plane III is given by

$$\vec{E}_{III} = \begin{bmatrix} E_{IIIp} \\ E_{IIIs} \end{bmatrix} = \begin{vmatrix} 1/\sqrt{2}\,\exp[j \cdot 3\pi/4] & 0 \\ 0 & 0 \end{vmatrix} \vec{E}_p + \begin{vmatrix} 1/\sqrt{2}\,\exp[j \cdot \pi/4] & 0 \\ 0 & 1 \end{vmatrix} \vec{E}_r \tag{15}$$

Consequently, the output signal S_p of the polarimeter detector results in

$$S_p = \vec{E}_{III} \vec{E}^{\times}_{III} = [\vec{E}_r \vec{E}^{\times}_r + E_{rs} E^{\times}_{rs} + E_{pp} E^{\times}_{pp}]/2 + \mathrm{Im}[E^{\times}_{pp} E_{rp}] \tag{16}$$

which can be written in the form

$$S_p = U_p + V_p \sin(\Delta\omega t + \Delta\varphi + \Phi_p) \tag{17}$$

Again, the quantities U_p, V_p, and Φ_p depend on the intensities and polarization parameters of the probing and reference waves, and for small polarization parameters we obtain approximately

$$U_p \approx (1 + 2\psi_r^2 + 2\varepsilon_r^2)\cdot I_r/2 + (\psi_p^2 + \varepsilon_p^2)\cdot I_p/2 \approx I_r/2$$
$$V_p \approx \sqrt{I_p I_r (\psi_p^2 + \varepsilon_p^2)} \qquad (18)$$
$$\tan \Phi_p \approx \varepsilon_p/\psi_p$$

So, the polarimeter detector yields a sinusoidal output signal whose amplitude is proportional to $\sqrt{\psi_p^2 + \varepsilon_p^2}$, and if we could employ a linearly polarized probing beam ($\varepsilon_p = 0$), then the amplitude V_p were a direct measure of the rotation angle. Unfortunately, some ellipticity due to plasma birefringence will be inevitable, but its influence is considerably reduced by using synchronous detection techniques as described in the following chapter.

III. Evaluation of detector signals

1. Interferometer signal

As already mentioned the arrangement described here is based on the interferometer developed by Véron /5/ for the TFR Tokamak. Consequently, the technique of phase shift measurement also follows the method given in ref. /5/. We briefly summarize it by refering to fig. 3. The heavy lines indicate a set up corresponding to fig. 1, in which the output signal of the detector D_I is given by equ. (13):

$$S_I = U_I + V_I \cos(\Delta\omega t + \Delta\varphi + \Phi_I)$$

The fine lines represent a second interferometer system without any plasma in its probing arm but using the same rotating grating for frequency shift. Its detector D_R provides a reference signal of the form

$$S_R = U_R + V_R \cos \Delta\omega t \qquad (19)$$

By comparing the oscillating components of S_I and S_R and measuring the time interval Δt between corresponding zero crossings the relative phase shift $(\Delta\varphi + \Phi_I)$ is found with high accuracy. Moreover, this technique yields the sign of phase shift variations and is independent from random amplitude fluctuations which may arise from refractive effects inside the plasma. On the other hand, the time resolution is correlated with the period of oscillation $\tau = 2\pi/\Delta\omega$, which has to be chosen smaller than the time scale variation of phase shift.

Since we are only interested in changes of phase shift relative to the situation before plasma ignition, we need not care about the constant phase angle Φ_1 (cf. the note in connection with equ. (14)). Using equ. (4) the electron line density along the probing beam path as a function of the measured time lag Δt results in:

$$\int_0^L N_e \cdot ds = -2{,}23 \cdot 10^{17} \frac{\Delta t}{\lambda \cdot \tau} + C \tag{20}$$

wherein the additive constant C takes into account the plasma-independent phase shift due to Φ_1. In practice, C is chosen in such a way that it compensates the first term of equ. (20) when there is no plasma in the probing arm.

2. Polarimeter signal

According to equ. (18) the amplitude V_p of the polarimeter signal is proportional to $\sqrt{\psi_p^2 + \varepsilon_p^2}$, and hence a graph of V_p versus ψ_p results in hyperbolas as shown in fig. 4 for different values of ε_p. Since the slope $dV_p/d\psi_p$ approaches zero at $\psi_p = 0$, exact measurements of small angles ψ_p are impossible. However, this difficulty may be overcome by introducing a constant bias angle ψ_{po} and thus shifting the range of measurement towards the quasi-linear parts of the hyperbolas (shaded section of fig. 4). In the arrangement of fig. 1 such a shift is readily done by slightly rotating the half-wave plate away from its 45^0 position. Nevertheless, one should keep in mind that the relation $V_p \sim \sqrt{\psi_p^2 + \varepsilon_p^2}$ is only valid for small polarization parameters (ψ ; ε), and shifting the range of measurement consequently impairs the approximations. To give an example, the amplitude V_p calculated from equ. (18) differs by ca. 4 % from the exact value, if the polarization parameters are supposed to be (ψ_p; ε_p) = (20^0; 0,1) and (ψ_r ; ε_r) = (5^0; 0,1). But this is not a real disadvantage since it can be eliminated by a suitable method of calibration (for example, by rotating the half-wave plate in well-defined steps and detecting the amplitude V_p as a function of the rotation angle). On the contrary, changes of ellipticity $\Delta\varepsilon_p$ due to variable linear birefringence may constitute a serious problem, if $\Delta\varepsilon_p$ is of the same order of magnitude as the variation $\Delta\psi_p$ of the rotation angle. In that case the calibration curve $V_p = f(\psi_p)$ is no longer a hyperbola as shown in fig. 4 but has to take into account the complicated relation between ellipticity and rotation angle. Fortunately, for typical TEXTOR parameters ($N_{eo} = 5 \cdot 10^{13}$ cm^{-3}; I = 300 kA; B_T = 2 T) and a probing wavelength of 337 μm the variation of ellipticity caused by linear birefringence amounts to less than $4 \cdot 10^{-3}$, which is small compared to the corresponding rotation angles (see chapter IV).

To measure the amplitude V_p with high accuracy, careful noise filtering of the polarimeter signal is absolutely necessary, esp. if room-temperature pyroelectric detectors are employed. To illustrate this requirement, we assume the power of the probing and reference beams to be $I_p = I_r = 5$ mW (which is a realistic value for a multichannel device), and we ask for a precision of $\Delta\psi_p = \pm 0{,}1$ deg. Then we must be able to resolve power variations in the order of a few μW. On the other hand, the noise equivalent power (NEP) of pyroelectric detectors (e.g. Mullard /17/, type 802 CPY) at a frequency of 10 kHz is about 10^{-8} W/$\sqrt{\text{Hz}}$. So, if we want a signal-to-noise ratio of 5, the detection bandwidth has to be restricted to a few kHz either by a suitable band-pass filter or - more effectively - by lock-in techniques. A lock-in amplifier gives an output voltage V_o, which is proportional to the amplitude V_T of the periodic test signal, when its reference input is fed with a signal of the same frequency:

$$V_o = V_T \cdot \cos \Phi_{TR} \tag{21}$$

where Φ_{TR} is the phase shift between the test and the reference signal. Noise signals adjacent to the reference produce a difference frequency output, which is attenuated according to the characteristics of the low-pass filter at the output of the lock-in amplifier. This results in an equivalent band-pass filter with a bandwidth equal to twice the low-pass cutoff frequency. Since in our case both the polarimeter signal (equ. (17)) and the interferometer signal (equ. (13)) have the same frequency and also experience the same phase shift $\Delta\varphi$ caused by plasma refractivity, we can use the latter as a reference. The output voltage is then given by

$$V_o = V_p \cdot \cos[\pi/2 - (\Phi_p - \Phi_I)] = V_p \cdot \sin(\Phi_p - \Phi_I) \tag{22}$$

Inserting the expressions for V_p, Φ_p, and Φ_I defined in equations (14) and (18) we arrive at

$$V_o = \sqrt{I_p I_r}\ \frac{\psi_p + \varepsilon_p - K(\psi_p^2 + \varepsilon_p^2)}{\sqrt{2 - 2K(\psi_p + \varepsilon_p) + K^2(\psi_p^2 + \varepsilon_p^2)}} \approx \sqrt{\frac{I_p I_r}{2}}\,(\psi_p + \varepsilon_p)\,. \tag{23}$$

It is interesting to note that V_o approximates to a linear function of ψ_p rather than a hyperbolic relation as was found for the amplitude V_p (cf. equ. (18)). So, the lock-in amplifier not only acts as a band-pass filter but also "linearizes" the dependence on the rotation angle and thus offers the additional chance to determine the sign of ψ_p.

Under real conditions, however, V_0 is not well suited for direct measurements of the rotation angle, because it depends on the intensities I_p and I_r of the probing and reference beam, which may fluctuate due to variations of the laser power and beam deviations caused by plasma refraction. For that reason it is necessary to eliminate the dependence on the intensities. This can be done by dividing the amplifier output V_0 by the amplitude V_I of the interferometer signal, since V_I is also proportional to $\sqrt{I_p I_r}$ (cf. equ. (14)). Fig. 5 summarizes the whole polarimeter data processing in the form of a block diagram (the high-pass filters are included in order to separate the dc parts from the detector signals; in case of pyroelectric detectors, which do not respond to constant intensities, the filters may be omitted). The output signal of the circuit results in

$$V_{out} = (V_p/V_I)\cdot\sin(\Phi_p - \Phi_I)\ . \tag{24}$$

Substituting the corresponding expressions and neglecting quadratic terms of ε_p and ψ_p, we obtain

$$V_{out} = \frac{1}{T_c - T_w}\ \frac{\psi_p + \varepsilon_p}{1 - K(\psi_p + \varepsilon_p)} \tag{25}$$

where T_c, T_w, and $K = (T_c + T_w)/(T_c - T_w)$ account for the transmission properties of the analyzer located in front of the interferometer detector. If $K(\psi_p + \varepsilon_p)$ is sufficiently small, we can further reduce equ. (25) to the simple linear relation

$$V_{out} = \frac{1}{T_c - T_w}\ [(1 + 2K\varepsilon_p)\psi_p + \varepsilon_p\ ]\ . \tag{26}$$

In order to estimate the error introduced by applying equ. (26) we compare it with the exact formula

$$V_{out} = \frac{2}{T_c - T_w}\cdot\frac{(1-\varepsilon_p^2)\sin\psi_p\cdot\cos\psi_p + \varepsilon_p - K(\sin^2\psi_p + \varepsilon_p^2\cos^2\psi_p)}{K^2(\sin^2\psi_p + \varepsilon_p^2\cos^2\psi_p) - 2K[(1-\varepsilon_p^2)\sin\psi_p\cdot\cos\psi_p + \varepsilon_p] + 2(\cos^2\psi_p + \varepsilon_p^2\sin^2\psi_p)}\ . \tag{27}$$

Fig. 6 shows some curves of V_{out} versus ψ_p calculated from both equations (26) and (27). The parameter K is supposed to be 1,05 corresponding to T_c = 90 % and T_w = 2 %. Within the range ($-15^0 < \psi_p < +15^0$) and ($-0{,}06 < \varepsilon_p < +0{,}06$) the angles ψ_p derived from the approximate curves differ by less than 8 % from the exact values. When the measuring range is restricted to ($-10^0 < \psi_p < +10^0$), the deviations become less than 5 %. Nevertheless, for high precision measurements one should take into account the non-linear relation between ψ_p and V_{out} by using the appropriate solid line of fig. 6 for calibration purposes.

In practice, this calibration curve is found by rotating the half-wave plate in front of the beam combiner (fig. 1) and detecting V_{out} as a function of the rotation angle.

Finally, we want to emphasize that the polarimetric technique described so far yields relevant results only if the ellipticity ε_p of the probing wave is a constant quantity, that is to say, variations of ε_p due to plasma birefringence must be negligible compared to changes of the rotation angle. This requirement is met by the TEXTOR plasma as will be shown in the following chapter.

IV. Calculation of polarization changes with regard to expected TEXTOR parameters

In order to evaluate the polarization changes of the probing beam we follow a work of Segre /18/, who derived a numerical method for calculating the output polarization as a function of plasma parameters. Segre's treatment is based on Appleton Hartree's formula for the refractive index μ of a magnetized plasma (e.g. Heald and Wharton /13/), and he uses the Stokes parameters for describing the state of polarization of an electromagnetic wave (e.g. Born and Wolf /19/). These parameters are defined by

$$\begin{aligned} s_1 &= \cos 2\chi \cdot \cos 2\psi \\ s_2 &= \cos 2\chi \cdot \sin 2\psi \\ s_3 &= \sin 2\chi \end{aligned} \tag{28}$$

where ψ is the angle between the major axis of the vibrational ellipse and a fixed coordinate axis (the p-axis of fig. 1). χ is related to the ellipticity ε by

$$\tan \chi = \varepsilon \; . \tag{29}$$

The Stokes parameters determine the polarization vector $\vec{s} = (s_1, s_2, s_3)$, which will change from point to point for a plane wave traversing a poloidal plasma cross section. If the scale length of gradients in the plasma is small compared to the radiation wavelength λ and if absorption and refractive beam deviations are negligible, the evolution of $\vec{s}$ can be represented by

$$\frac{d\vec{s}}{dz} = \vec{\Omega}(z) \times \vec{s}(z) \tag{30}$$

where z denotes the direction of propogation of the probing wave. The vector $\vec{\Omega}$ (z) contains the wave frequency $\omega = 2\pi c/\lambda$ and the plasma parameters and is given by

$$\vec{\Omega}(z) = \frac{\omega}{c} [\mu_1(z) - \mu_2(z)] \cdot \vec{s}_{c2}(z). \tag{31}$$

μ_1 and μ_2 are the refractive indices and $\vec{s}_{c1}$ and $\vec{s}_{c2}$ are the polarization vectors of the slow and fast characteristic waves, resp. (characteristic waves do not change their state of polarization; for a magnetized plasma it can be shown that for each direction of propagation there exist two elliptically polarized characteristic waves which are related by $\psi_2 = \psi_1 + \pi/2$ and $\varepsilon_2 = -\varepsilon_1$).

To solve equ. (30) Segre introduces the dimensionless variables $X = x/r$ and $Z = z/r$ (see fig. 7). Furthermore, he supposes that the electron density N_e and the current density j only depend on the dimensionless radius $R = \sqrt{X^2 + Z^2}$ (this assumption considerably simplifies the calculations though it may not quite conform to the actual situation in a Tokamak plasma; nevertheless, the results indicate at least the order of magnitude of ellipticity caused by the plasma). The radial distributions of electron density and poloidal magnetic field are expressed by the functions f(R) and b(R):

$$N_e(R) = N_{eo} f(R)$$

$$B_p(R) = \frac{4\pi}{Rc} \int_0^R j(R')\, R'\, dR' = B_I \cdot b(R) \tag{32}$$

where N_{eo} is the central density; B_I is the poloidal field at the plasma edge which is a function of the plasma current I:

$$B_I = B_p(R=1) = \frac{2I}{rc}. \tag{33}$$

The toroidal magnetic field B_T normal to the probing beam path depends on the distance from the torus axis. If B_{To} is the central value at $X = 0$ and α denotes the ratio of minor to major radius of the torus, then

$$B_T(X) = \frac{B_{To}}{1 + \alpha X}. \tag{34}$$

Introducing the vector $\vec{T} = r\vec{\Omega}$ and substituting the refractive indices and the polarization vector $\vec{s}_{c2}$ in equ. (30) Segre finally arrives at the following system of three equations:

$$\frac{ds_1}{dZ} = T_2(Z)\cdot s_3(Z) - T_3(Z)\cdot s_2(Z)$$

$$\frac{ds_2}{dZ} = T_3(Z)\cdot s_1(Z) - T_1(Z)\cdot s_3(Z) \qquad (35)$$

$$\frac{ds_3}{dZ} = T_1(Z)\cdot s_2(Z) - T_2(Z)\cdot s_1(Z)$$

where the vector components are given by

$$T_1 = \frac{PQU}{D(\mu_1+\mu_2)}\cdot\frac{Q^2[X^2+Z^2]-[Z\cdot b(Z)]^2}{Q^2[X^2+Z^2]\cdot[1-N_o\cdot f(Z)]}\cdot f(Z)$$

$$T_2 = \frac{2PU}{D(\mu_1+\mu_2)}\cdot\frac{Z\cdot f(Z)\cdot b(Z)}{\sqrt{X^2+Z^2}\,[1-N_o\cdot f(Z)]} \qquad (36)$$

$$T_3 = \frac{2P}{D(\mu_1+\mu_2)}\cdot\frac{X\cdot f(Z)\cdot b(Z)}{\sqrt{X^2+Z^2}}$$

with

$$D = 1 - \frac{U^2}{Q^2[X^2+Z^2]}\cdot\left[[X\cdot b(Z)]^2 + \frac{Q^2[X^2+Z^2]+[Z\cdot b(Z)]^2}{1-N_o\cdot f(Z)}\right] \qquad (37)$$

The quantities N_o, P, U, and Q represent physical parameters whose values are calculated from the following expressions:

$$N_o = 0{,}889\cdot 10^{-13}\lambda^2 N_{eo}$$

$$P = 1{,}036\cdot 10^{-14}\lambda^2 N_{eo}\,I$$

$$U = 0{,}934\,\lambda B_T \qquad (38)$$

$$Q = 50\,r B_T/I$$

(λ and r in cm, N_{eo} in cm^{-3}, I in kA, B_T in Tesla).

The system of equations (35) can be integrated numerically by dividing the probing beam path into a series of uniform sections (Z; $Z + \Delta Z$). The integration starts at $Z = -Z_o = -\sqrt{1-X^2}$ with an initial polarization vector $\vec{s}_o = (s_{10}, s_{20}, s_{30})$ and ends at $Z = +Z_o$. The resulting output value of $\vec{s}$ gives the orientation ψ of the vibrational ellipse and its ellipticity ε:

$$\psi = \frac{1}{2}\arctan(s_2/s_1)$$

$$(39)$$

$$\varepsilon = \frac{s_3}{1+\sqrt{1-s_3^2}}$$

We will now apply this method to a probing beam of 337 μm wavelength traversing a poloidal cross section of the TEXTOR plasma at different positions X. Our numerical calculations include the dependence of B_T on X according to equ. (34), but we neglect N_o and put the sum of refractive indices $\mu_1 + \mu_2$ = const = 2 in equ. (36) (the former is permitted because $N_o < 10^{-2} \ll 1$ for central densities up to 10^{14} cm^{-3}, and the latter is tolerable since $\mu_1 + \mu_2$ varies by less than 1 % within the range of interest). For both the electron and current densities we assume parabolic distributions

$$\begin{aligned} N_e(R) &= N_{eo} \cdot (1 - R^2) \\ j(R) &= j_o \cdot (1 - R^2) \end{aligned} \tag{40}$$

which corresponds to

$$\begin{aligned} f(R) &= (1 - R^2) = (1 - X^2 - Z^2) \\ b(R) &= 2R - R^3 = \sqrt{X^2 + Z^2}\,(2 - X^2 - Z^2) \end{aligned} \tag{41}$$

We use the following set of parameters appropiate to the TEXTOR Tokamak:

central density	$N_{eo} = 5 \cdot 10^{13}$ cm^{-3}
plasma current	$I = 300$ kA
toroidal field	$B_T = 2$ T
$\frac{\text{minor radius}}{\text{major radius}}$	$\alpha = 0{,}286$

Based on these data the numerical integration of equ. (35) is carried out with a stepwidth of $\Delta Z = 0{,}02$. Fig. 8 shows the results for different initial polarization vectors $\vec{s}_o$. The curves marked by I result from linear input polarization parallel to B_T, and the curves labelled II correspond to elliptical input polarization ($\varepsilon_o = 0{,}05$) orientated at 5^0 with respect to B_T (note, that this choice is inadequate to the schematic lay-out shown in fig. 1, but it conforms to the actual arrangement planned for TEXTOR). In fig. 8a the rotation angles are plotted versus the probing beam distance X from the plasma center. The dashed line attached to curve II represents the situation that linear birefringence caused by both the toroidal field B_T and the poloidal component $B_\perp$ normal to the probing beam is completely neglected. A corresponding formula is derived from equ. (1) by substituting $B_\parallel = (X/R) \cdot B_p(R)$ and $N_e(R)$ according to our assumptions (32) and (41):

$$\psi(X) = 7{,}99 \cdot 10^{-14} \cdot \lambda^2 \cdot N_{eo} \cdot I \cdot X \cdot \sqrt{1 - X^2}\,(4X^4 - 13X^2 + 9) \tag{42}$$

(ψ in deg, λ in cm, N_{eo} in cm^{-3}, I in kA).

The difference between both graphs (II) demonstrates a marked influence of transverse magnetic fields on the rotation angle. On the other hand, for linearly polarized input waves (I) the approximation (42) coincides with the numerically calculated values within the accuracy of drawing in fig. 8a (the difference is less than 0,03 deg). So, the analytic expression (1), which considerably simplifies the evaluation of measured rotation angles, should be used only for linear input polarization parallel to B_T. In that case, however, it yields rather accurate results also for non-parabolic distributions $N_e(R)$ and j(R), as was proved in a series of comparative calculations.

Fig. 8b shows the changes of ellipticity $\Delta\varepsilon$ experienced by the probing waves. The asymmetry of the curves depends on the signs of B_T and I and is due to the fact that the angle between the plane of polarization and the total transverse field is either increased or decreased by Faraday rotation in the inner and outer half of the plasma cross section. Again, linear input polarization parallel to B_T (curve I) is favourable, since it reduces $\Delta\varepsilon$ to less than $4 \cdot 10^{-3}$. In terms of the polarimeter signal (equ. (26)) this value corresponds to an output error of 0,22 deg or 6,5 % at the probing beam position X = -0,4, and this percentage error is not exceeded at any other position.

V. Conclusion

A method for combined measurements of the line integrals $\int N_e ds$ and $\int N_e \cdot B_{\parallel} \cdot ds$ appropiate to the TEXTOR Tokamak has been described. Concerning the line density $\int N_e ds$ an experimental accuracy of about 10^{-2} interferometric fringes or $\Delta \int N_e ds < 10^{13}$ cm^{-2} can be achieved with a carefully designed set up (Véron et.al. /5/). For a typical beat frequency of $\Delta\omega$ = 10 kHz the time resolution is 100 μs. The sensitivity of Faraday rotation measurements yielding $\int N_e \cdot B_{\parallel} \cdot ds$ is mainly restricted by the influence of linear plasma birefringence and by detector noise. Using lock-in techniques an accuracy of 10 - 15 % should be possible with a time resolution of several milliseconds.

Extended to a multichannel arrangement the method offers a chance to determine the electron density distribution and the current density profile for the complete duration of the Tokamak discharge. However, the problems connected with the inversion of measured data to wanted profiles are difficult even for high experimental accuracy (e.g. Kunz /20/). Therefore, a final valuation of the method requires detailed tests under real Tokamak conditions.

Acknowledgements

The author is greatly indebted to Dr. D. Vēron and Dr. J.P. Crenn, Ass. EURATOM-CEA sur la Fusion, Fontenay-aux-Roses, for many valuable suggestions and fruitful discussions.

References

/1/ Vēron, D.
CEN Fontenay-aux-Roses, report nr. EUR-CEA-FC-980 (1978)

/2/ De Marco, F., Segre, S.E.
Plasma Phys. 14 , 245 (1972)

/3/ Belland, P., Vēron, D., Whitbourn, L.B.
Journ. Phys. D 8, 2113 (1975)
Appl. Optics 15, 3047 (1976)

/4/ Peacock, N.J.
"Measurement of Magnetic Fields in Toroidal Systems",
in: Diagnostics for Fusion Experiments, Varenna 1978,
Eds. Sindoni, E., Wharton, C., Pergamon Press, Oxford 1979

/5/ Vēron, D., Certain, J., Crenn, J.P.
J. Opt. Soc. Am. 67, 964 (1977)

/6/ Andrade, O.
Appl. Optics 15, 1378 (1976)

/7/ Kunz, W., Equipe TFR
Nuclear Fusion 18, 1729 (1978)

/8/ Pieroni, L.
CNEN Frascati, report nr. 77.25/cc (1977)

/9/ Dodel, G., Kunz, W.
Plasma Phys. 20, 171 (1978)

/10/ Dodel, G., Kunz, W.
Infrared Physics 18, 773 (1978)

/11/ Vêron, D.
Optics Communications 10, 95 (1974)

/12/ Alpher, R.A., White, D.R.
"Optical Interferometry" in: Plasma Diagnostic Techniques, Eds. Huddlestone, R.H., Leonard, S.L., Academic Press, New York 1965

/13/ Heald, M.A., Wharton, C.B.
"Plasmadiagnostics with Microwaves", John Wiley, New York 1965

/14/ Marcuvitz, N.
"Waveguide Handbook", McGraw-Hill, New York 1951

/15/ Möller, K.D., Rothschild, W.G.
"Far-Infrared Spectroscopy", John Wiley, New York 1971

/16/ SPECAC Analytical Accessories Ltd, Unit 3, Lagoon Road, St. Mary Cray, Orpington, Kent BR5 3QX, Great Britain

/17/ Mullard Ltd, Mullard House, Torrington Place, London WC 1E 7 HD, Great Britain

/18/ Segre, S.E.
Plasma Phys. 20, 295 (1978)

/19/ Born, M., Wolf, E.
"Principles of Optics", Pergamon Press, Oxford 1964

/20/ Kunz, W.
Thesis, Universität Stuttgart, 1979

Figure captions

Fig. 1: Schematic layout of the combined interferometric and polarimetric diagnostics

Fig. 2: Characteristics of the wire grid beam combiner

Fig. 3: Principle of phase shift measurement

Fig. 4: Polarimeter detector amplitude versus rotation angle for different probing wave ellipticities

Fig. 5: Block diagram for the polarimeter data processing

Fig. 6: Polarimeter output signal versus rotation angle for different probing wave ellipticities

Fig. 7: Definition of coordinates for the numerical calculation of polarization changes

Fig. 8: rotation angle and change of ellipticity versus probing beam position

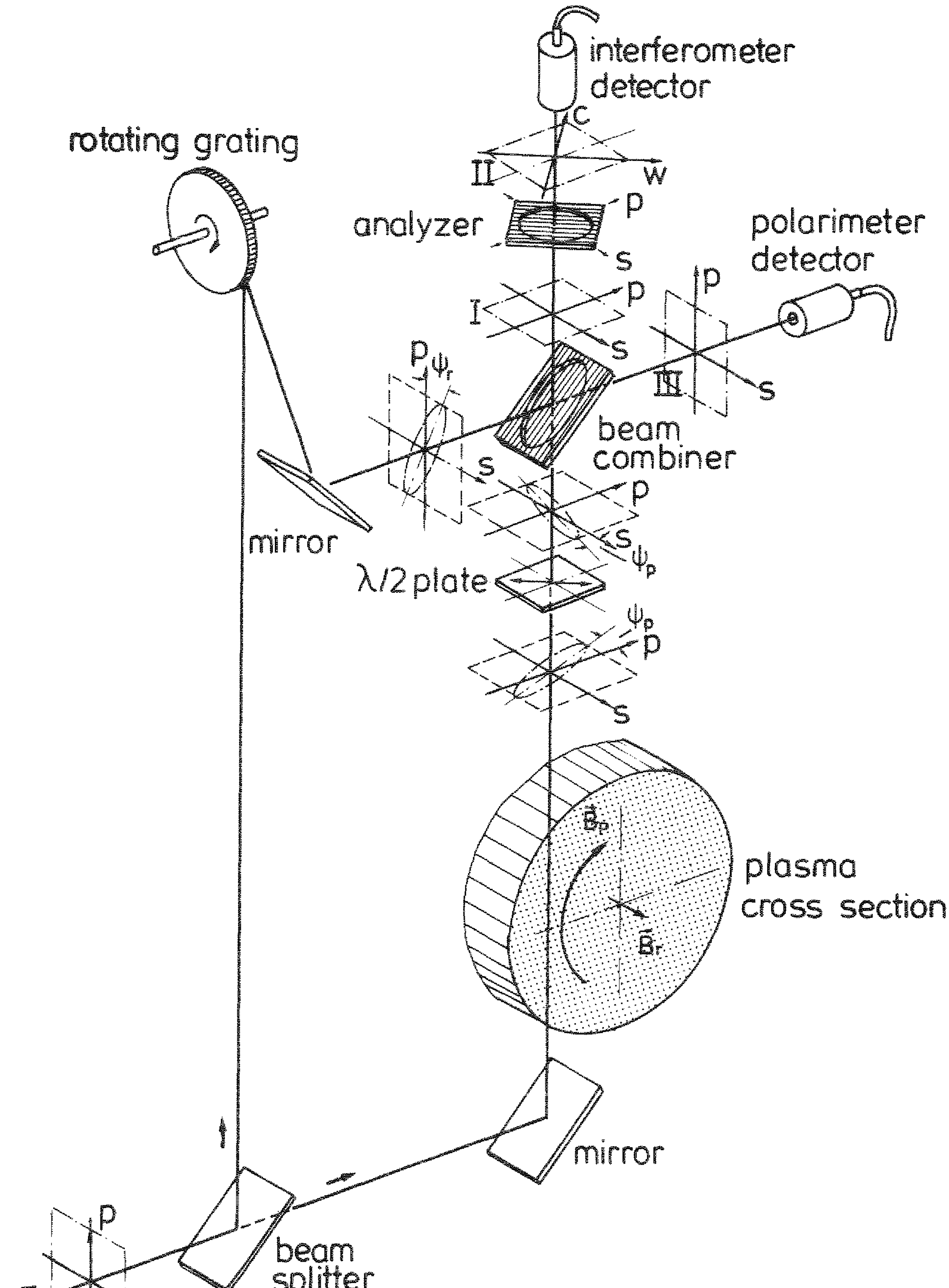
interferometer
detector
c
II
w
rotating grating
analyzer
p
s
polarimeter
detector
I
p
s
p
III
s
P_{ψ_r}
beam
combiner
s
p
s
ψ_p
mirror
λ/2 plate
ψ_p
p
s
$\vec{B}_p$
plasma
cross section
$\vec{B}_r$
mirror
p
beam
splitter
s

Fig.1

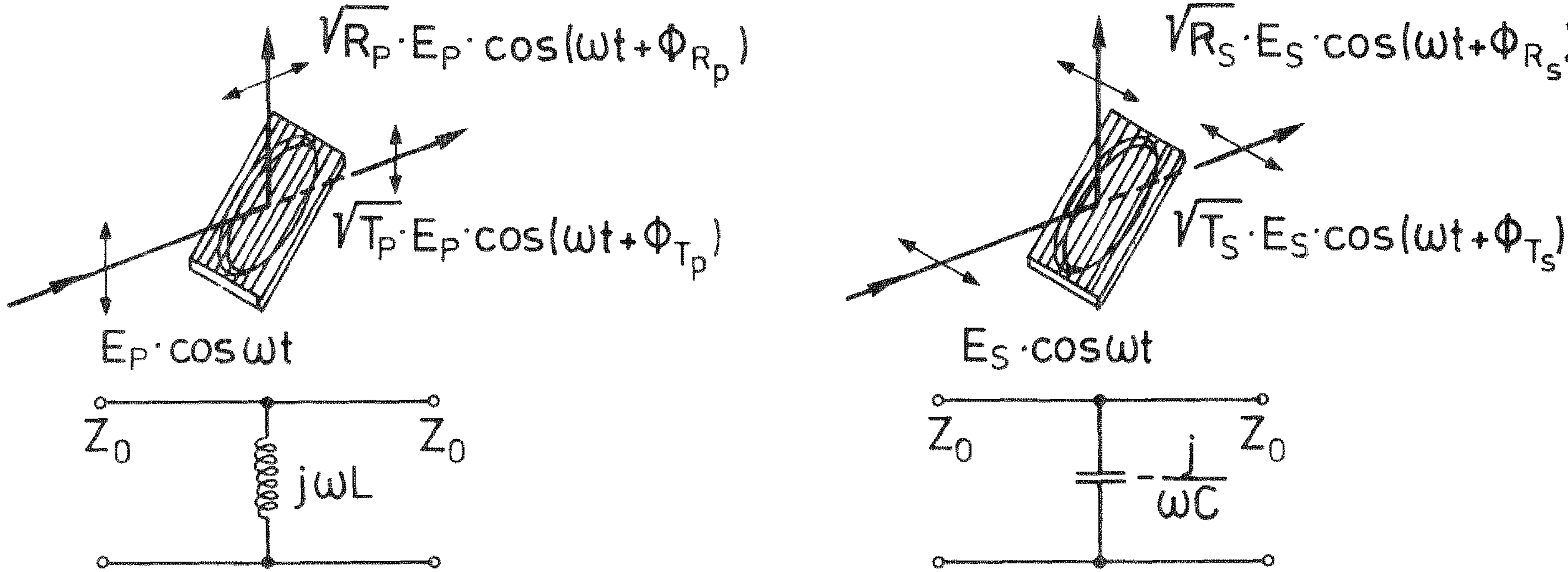

$$\frac{\omega L}{Z_0} = \frac{1}{2}$$

$$R_P = \frac{1}{2} \; ; \; T_P = \frac{1}{2}$$

$$\Phi_{R_p} = \frac{3}{4}\pi \; ; \; \Phi_{T_p} = \frac{1}{4}\pi$$

inductive wire grid

$$\frac{1}{\omega C Z_0} \gg 1$$

$$R_S \ll 1 \; ; \; T_S \approx 1$$

$$\Phi_{R_s} \approx -\frac{\pi}{2} \; ; \; \Phi_{r_s} \approx 0$$

capacitive wire grid

Fig. 2

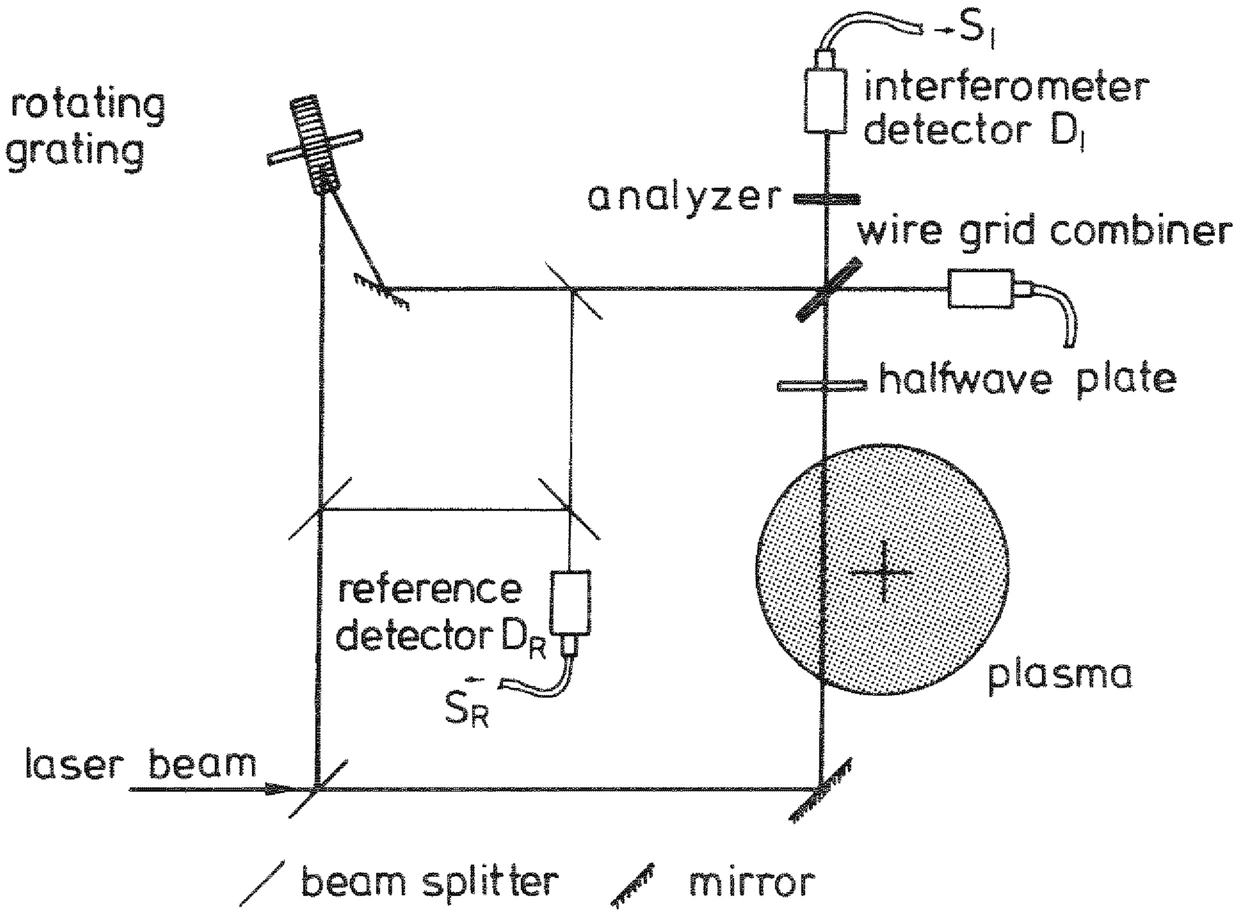

$\to S_I$
interferometer detector D_I
rotating grating
analyzer
wire grid combiner
halfwave plate
plasma
reference detector D_R
S_R
laser beam
beam splitter
mirror

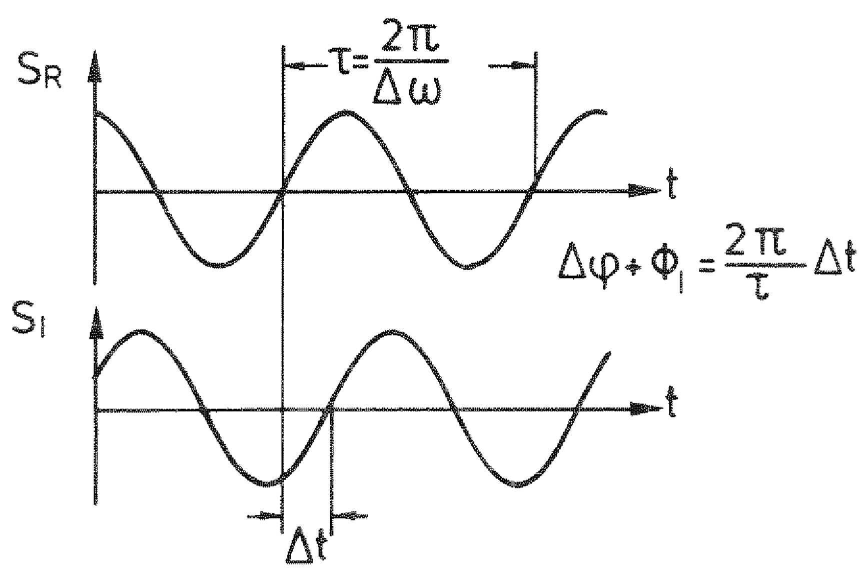

S_R
$\tau = \frac{2\pi}{\Delta\omega}$
t
$\Delta\varphi + \Phi_I = \frac{2\pi}{\tau}\Delta t$
S_I
t
Δt

Fig. 3

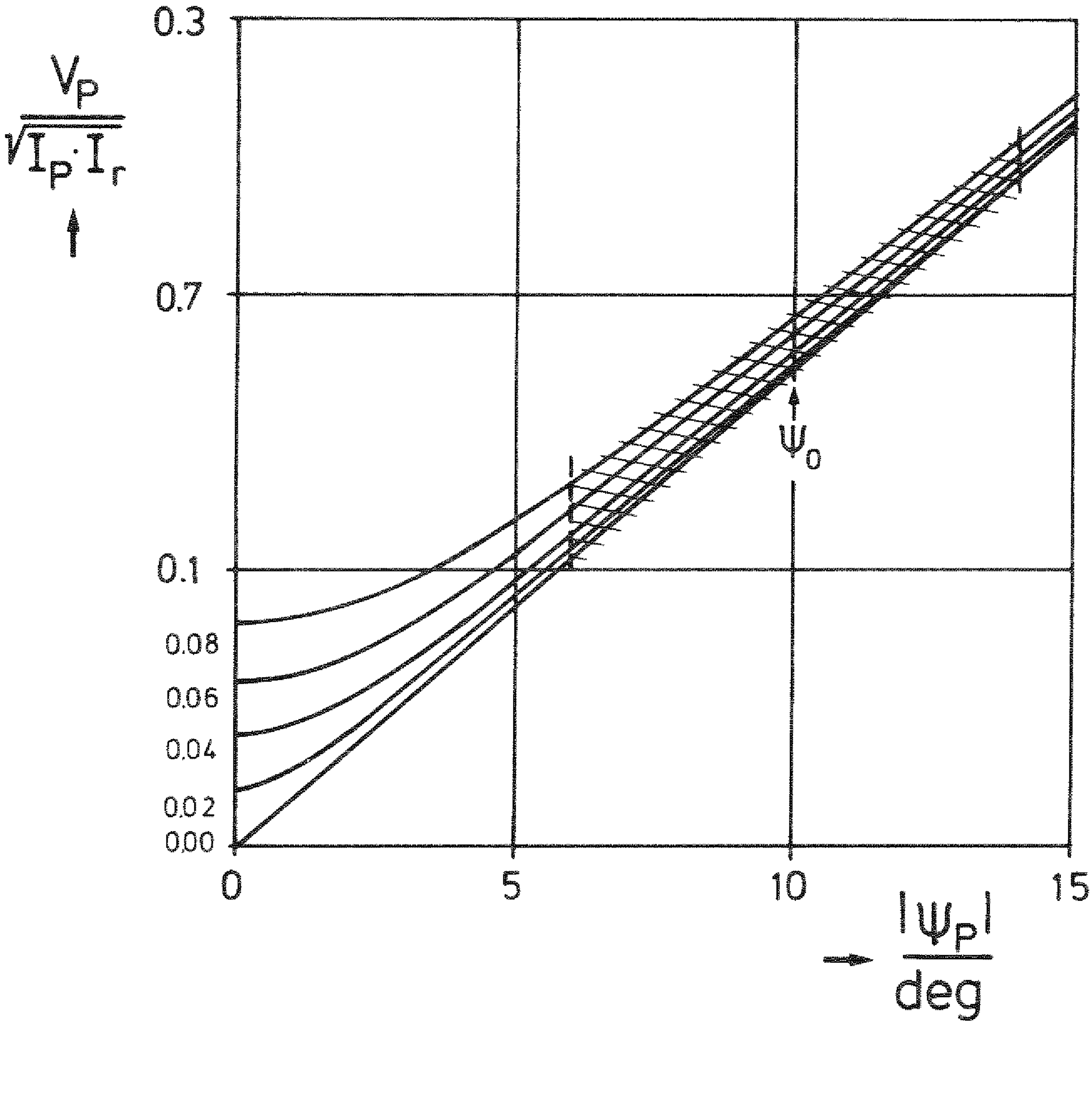

0.3
$\frac{V_P}{\sqrt{I_P \cdot I_r}}$
0.7
0.1
0.08
0.06
0.04
0.02
0.00
ψ_0
0
5
10
15
$\frac{|\psi_P|}{deg}$

Fig.4

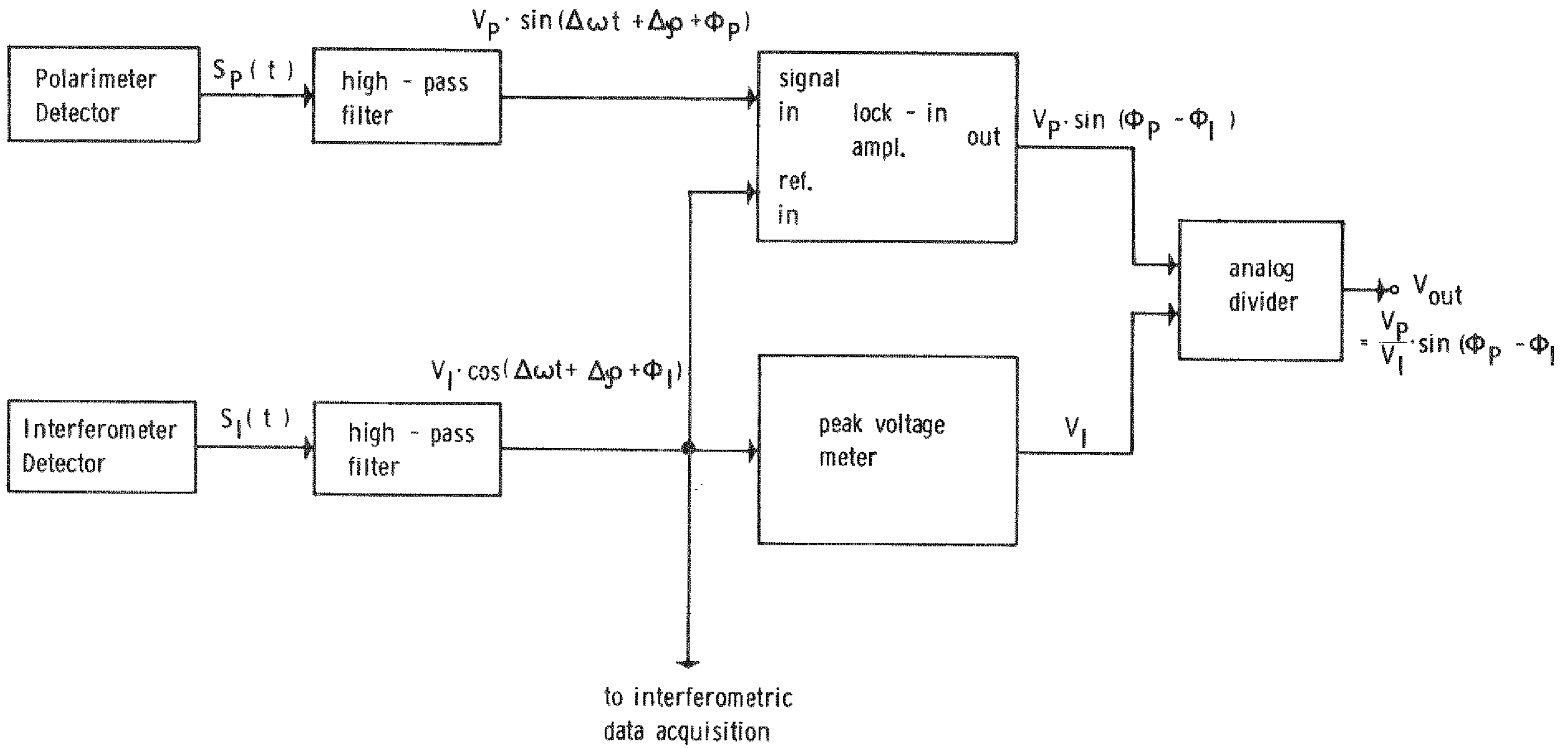

Polarimeter Detector
$S_P(t)$
high - pass filter
$V_P \cdot \sin(\Delta\omega t + \Delta\varphi + \Phi_P)$
signal in
lock - in ampl.
out
ref. in
$V_P \cdot \sin(\Phi_P - \Phi_I)$
analog divider
$V_{out} = \frac{V_P}{V_I} \cdot \sin(\Phi_P - \Phi_I)$
Interferometer Detector
$S_I(t)$
high - pass filter
$V_I \cdot \cos(\Delta\omega t + \Delta\varphi + \Phi_I)$
peak voltage meter
V_I
to interferometric data acquisition

Fig.5

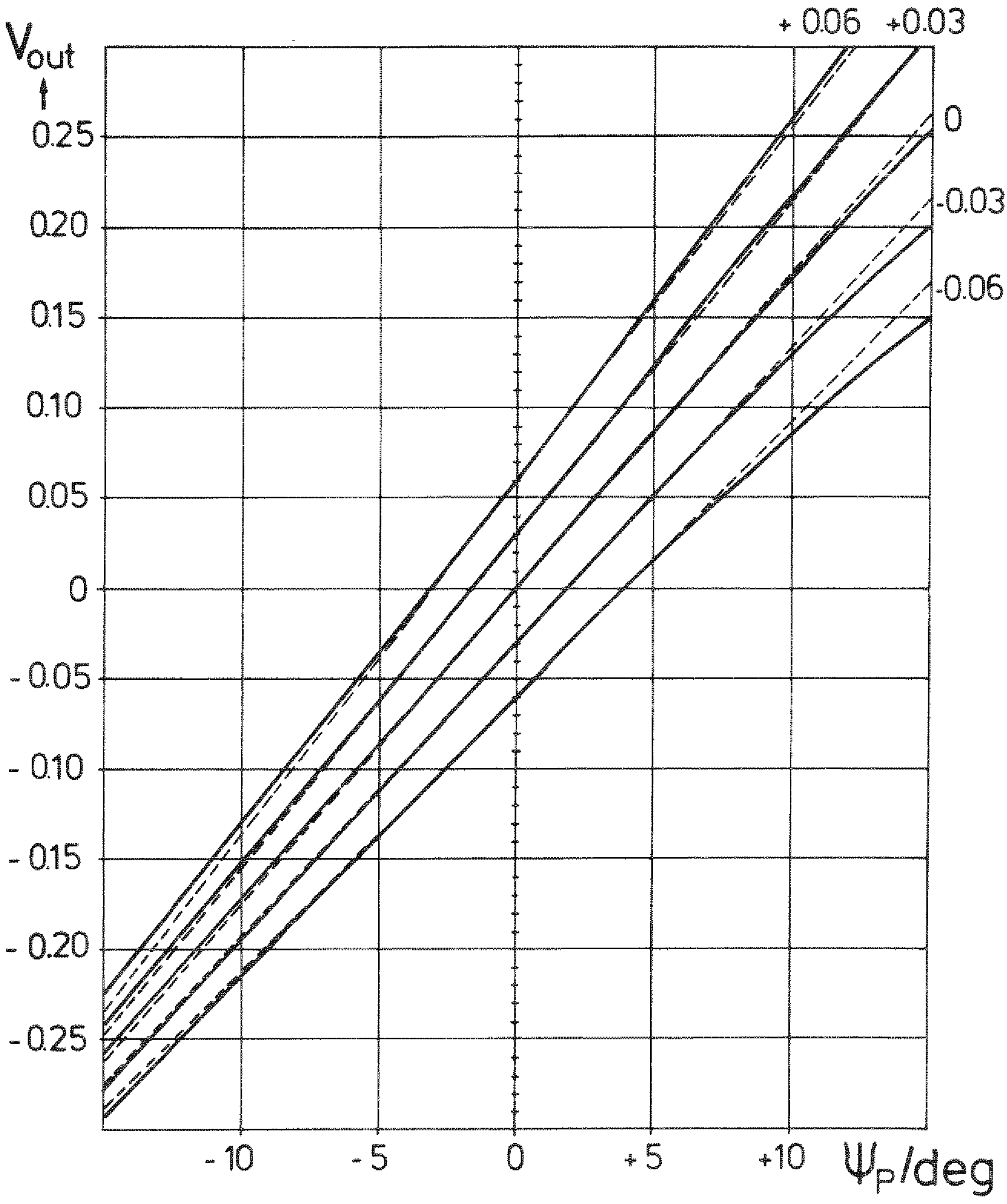
V_{out}
0.25
0.20
0.15
0.10
0.05
0
- 0.05
- 0.10
- 0.15
- 0.20
- 0.25
- 10
- 5
0
+ 5
+ 10
Ψ_P/deg
+ 0.06
+ 0.03
0
-0.03
-0.06

Fig. 6

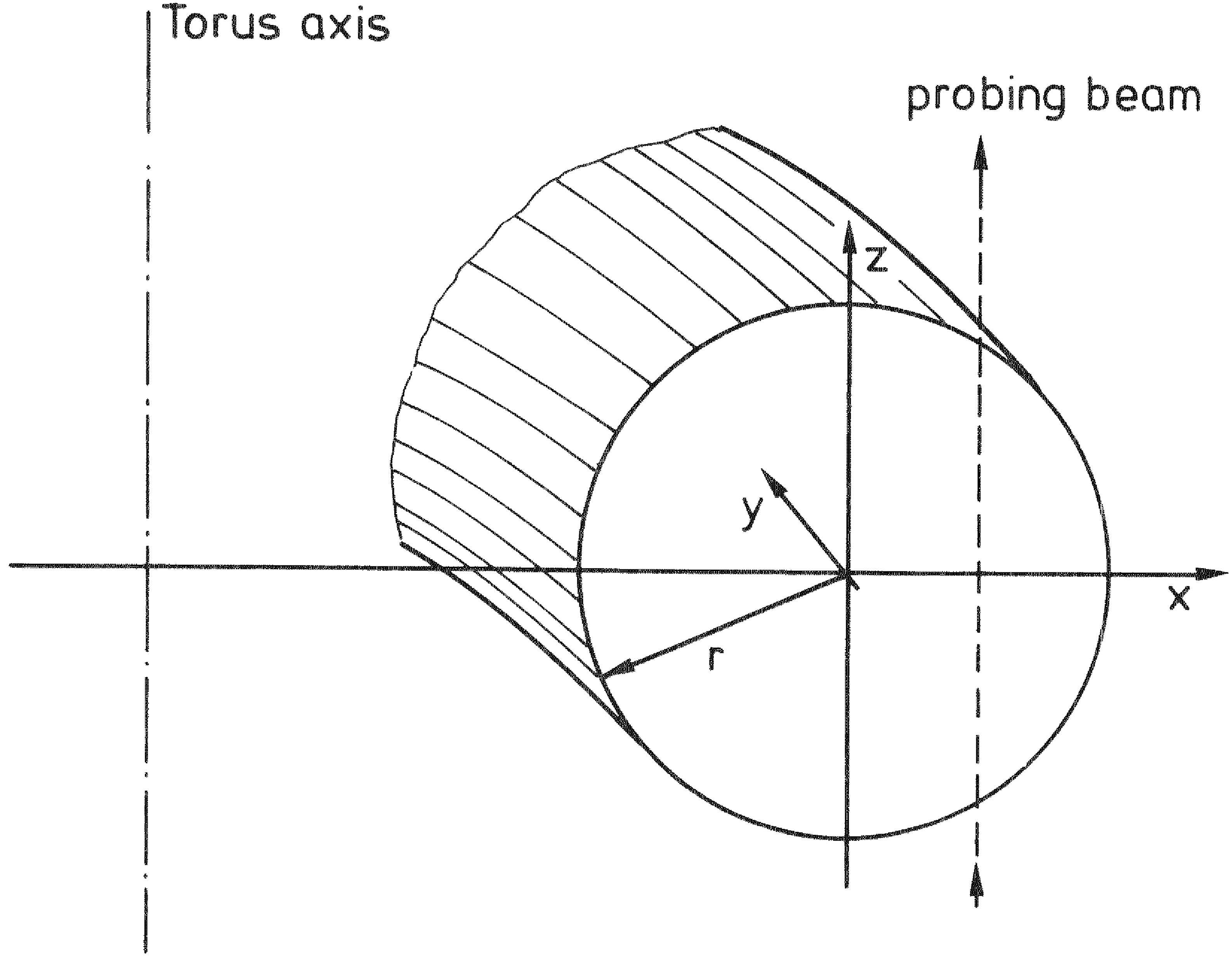

Fig. 7

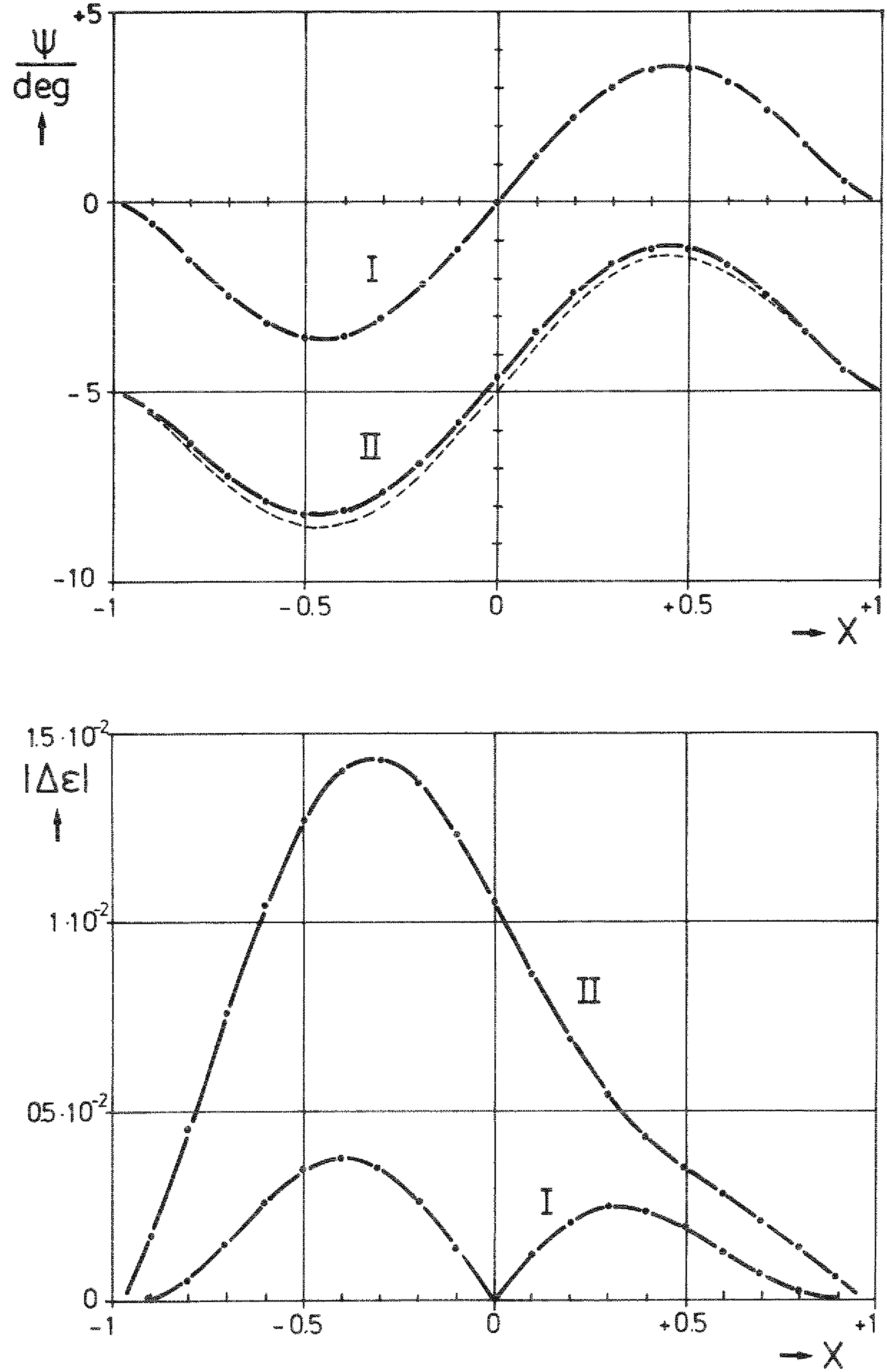

$\frac{\psi}{\text{deg}}$
+5
0
-5
-10
-1
-0.5
0
+0.5
+1
X
I
II
$1.5 \cdot 10^{-2}$
$|\Delta\varepsilon|$
$1 \cdot 10^{-2}$
$0.5 \cdot 10^{-2}$
0
-1
-0.5
0
+0.5
+1
X
II
I

Fig. 8